





Article

# Development of Optimization Based Control Strategy for P2 Hybrid Electric Vehicle including Transient Characteristics of Engine

Gulnora Yakhshilikova <sup>1,\*</sup>, Sanjarbek Ruzimov <sup>1,2</sup>, Ethelbert Ezemobi <sup>1</sup>, Andrea Tonoli <sup>1</sup>  
and Nicola Amati <sup>1</sup>

<sup>1</sup> Department of Mechanical and Aerospace Engineering, Politecnico di Torino, 10129 Torino, Italy; sanjarbek.ruzimov@polito.it (S.R.); ethelbert.ezemobi@polito.it (E.E.); andrea.tonoli@polito.it (A.T.); nicola.amati@polito.it (N.A.)

<sup>2</sup> Department of Mechanical and Aerospace Engineering, Turin Polytechnic University in Tashkent, Tashkent 100095, Uzbekistan

\* Correspondence: gulnora.yakhshilikova@polito.it

**Abstract:** Models based on steady-state maps estimate fuel consumption to be 2–8% lower than real experimental measured values. This is due to the fact that during transient phases, the engine consumes more fuel than in steady phases. Some literature has addressed the conventional vehicle engine model that improves fuel consumption estimation's accuracy during the transient state. However, the characteristics of the engine in the scope of hybrid electric vehicles (HEVs) with an integrated control strategy is yet to be covered. The controller is designed to minimize engine operation in the transient phase to enhance energy savings. In this paper, the correlation between fuel enrichment in transient and steady-state fuel estimation is established as transient correction factor (TCF). Its explanatory variable was the engine torque change rate. This paper describes the influence of engine transient characteristics on the fuel consumption of a mild HEV. The work attempts to improve the fuel economy of the HEV by introducing a penalty factor in the controller to optimize the use of the engine in transient regimes. A backward vehicle model was developed for a production vehicle with a conventional powertrain and validated experimentally using data available online. The corresponding hybrid vehicle model was developed by integrating the electric motor and battery components with the conventional vehicle model. A P2 off-axis configuration was chosen to this end as the HEV architecture. A conventional equivalent consumption minimization strategy (ECMS) was used to split the torque request between the engine and the electric motor. This control strategy was modified with TCF to penalize the engine torque change rate. The results of the simulation show that due to less transient operation of the engine, the fuel consumption was reduced from 923 g to 918 g under the US06 driving cycle. The fuel economy of the model has been simulated for UDDS and HW drive cycles too, and fuel consumption improved by 4.4 g and 3.2 g, respectively. It has been verified that by increasing the battery capacity twice (14s24p), the limitations imposed by the battery capacity can be minimized and the fuel usage can be reduced by 9 g in the UDDS cycle.

**Keywords:** transient fuel consumption model; equivalent consumption minimization strategy; mild hybrid electric vehicle



**Citation:** Yakhshilikova, G.; Ruzimov, S.; Ezemobi, E.; Tonoli, A.; Amati, N. Development of Optimization Based Control Strategy for P2 Hybrid Electric Vehicle including Transient Characteristics of Engine. *Appl. Sci.* **2022**, *12*, 2852. <https://doi.org/10.3390/app12062852>

Academic Editor: Adel Razek

Received: 20 January 2022

Accepted: 7 March 2022

Published: 10 March 2022

**Publisher's Note:** MDPI stays neutral with regard to jurisdictional claims in published maps and institutional affiliations.



**Copyright:** © 2022 by the authors. Licensee MDPI, Basel, Switzerland. This article is an open access article distributed under the terms and conditions of the Creative Commons Attribution (CC BY) license (<https://creativecommons.org/licenses/by/4.0/>).

## 1. Introduction

Improving fuel efficiency and reducing the greenhouse emissions of vehicles has become crucial in the automotive industry. A wide range of technologies is used to this end. In [1], simple models are developed to estimate the subsystems' steady-state performances and efficiency of the entire vehicle. The models are combined to simulate the vehicle behavior for different driving cycles and assess the fuel economy for the effect of design variations and new technologies. In [2], fuel saving was achieved by adjusting vehicle

height, using an electromechanical system which results in reduced aerodynamic resistance of the vehicle.

An interest in electrification of the powertrain, i.e., using hybrid electric vehicles (HEV), as a means of improving fuel efficiency and minimizing greenhouse emissions is growing rapidly [3]. By adding an electric motor (EM) in parallel to the internal combustion engine (ICE), it is possible to recover the braking energy, store it in the battery, and use it later during the traction phase. Furthermore, ref. [4] introduced an ELPH (electrically peaking hybrid) control strategy that offers EM power usage for acceleration and deceleration phases, whereas ICE provides mean load power of the driving cycle. The main aim of this logic is to use ICE at high speeds with smooth torque demand.

A great deal of research and practical work has attempted to model the performance of the HEVs for optimizing their efficiency. In most of these works, the vehicle simulation models utilized the steady-state maps of the ICE to estimate fuel consumption [3,5]. It has been observed that measured fuel consumption data shows a higher value with respect to one calculated using the steady-state maps. This is due to the higher fuel consumption of the engine during transient phases. In [6], the measured fuel consumption was compared to that calculated with steady-state fuel consumption maps as a function of measured torque and speed of the ICE. Testing two vehicles, such as a Chevrolet Silverado with a 4.3 L Ecotec engine and a Ford F-150 with a 2.7 L EcoBoost engine, they concluded that the difference, due to transient fuel consumptions, was in the range of 2–4%. Furthermore, they established that more aggressive driving conditions could increase this range due to increased transient contribution. Certainly, this difference depends not only on the driving cycle but also on the vehicle parameters and the engine type. Various engines with 3.8 L to 8 L displacement were studied in [7], demonstrating that on different drive cycles, the fuel enrichment due to transient phenomena varied by 2–8%.

A relatively wide range of literature describes different approaches to model the engine transient behavior that estimates precisely the fuel consumption under different operating conditions and for different applications [6–12]. The authors of [6] considered four transient events, such as powertrain torque management (during the gear upshift phase for shafts synchronization), tip-in demand, deceleration fuel cutoff, and cylinder deactivation. The influence of each event on the transient fuel rate has been analyzed using experimental data. The corresponding adjustments have been applied to the steady-state fuel consumption to obtain the transient one. In [8], to produce an engine map that includes transient behavior, the engine torque and speed range was divided into equal bins. Then, the experimentally measured fuel consumption data was allocated to the bins to determine a representative value for each bin. The probability distribution function was analyzed and based on this data, the corresponding engine map was created. Fuel consumption prediction was improved relative to steady-state calculation in [9] by applying the correction factor, which is function of torque, speed, and power change rates. In [10], the vehicle fuel consumption was separated into two modes: cruising at a constant speed and acceleration operating modes. In each of these modes, the fuel consumption was calculated based on the instantaneous engine efficiency, approximated using an analytical function rather than the fuel consumption map. In [11], a real-time prediction of the fuel consumption was evaluated as first order linear function that varies with VSP (vehicle specific power). The analysis in [12] used vehicle speed ( $v$ ) and acceleration ( $a$ ) as dynamic variables to provide the transient correction to be added to the steady-state predicted value. The sign of VSP was used to choose a form of the correction factor.

The model proposed by [12] was used as a reference in [13] and further improved taking into account the computational time and accuracy of the model. In [14], engine torque and rotation speed are used as dynamic variables. Four different cases were considered, depending on the sign of engine torque and rotation speed change rate. A correction factor was then applied to multiply the steady-state fuel consumption. The approach was convenient to compute the fuel consumption of a vehicle in transient conditions using a backward model.

The abovementioned transient corrections were performed on a vehicle with conventional powertrains to improve the accuracy of fuel consumption computation using steady-state maps. As to the authors' knowledge, no attempt was made to study the improvement of the control strategy of the HEVs by integrating the transient correction of the engine fuel consumption.

In HEV applications, the improved accuracy of fuel consumption computation allows for further optimization of the torque split between EM and ICE. Equivalent fuel consumption minimization strategy (ECMS) is an online optimization-based strategy. Due to its online feature, the ECMS controller can define an optimal ratio of torque split at each instant of time, hence acting as a real-time controller. The ECMS was first applied by Paganelli et al. to HEV [15], where a concept of conversion of the battery energy to equivalent fuel consumption was introduced. The equivalence factor had a substantial effect on the overall efficiency of the HEV. A genetic algorithm was used in [16] for optimal selection of the equivalence factor. ECMS allows for penalizing battery use in case of its undesired state of charge (SOC), temperature, and degradation to maintain the desired operating conditions of the battery [17–19]. However, the penalization of the ICE use in transient operations cannot be found in the literature.

To fill this gap, this paper proposes an approach to reduce the fuel consumption of HEVs in transient phases by imposing a transient correction factor (TCF) proposed in [14] in the control strategy. The objective function to be minimized included TCF as a function of a torque changing. The electric machine can deliver torque quickly and with a minor efficiency variation over the operating range. Hence, the best mode to manage the torque transients is to rely more on the EM. An advantage of this approach is the possibility to reduce extra fuel consumption of the ICE in transient phases. Hence, the contributions of the paper comprise the model of the P2 HEV that includes the transient fuel correction and the developed control strategy to reduce fuel consumption by exploiting the e-motor more in transient phases.

The paper is organized as follows. First, the backward model of the HEV longitudinal dynamics and fuel consumption model is briefly described. Then, the transient fuel consumption model and its experimental validation based on experimental data available online [20,21] are reported. The TCF is introduced in the ECMS objective function. The results obtained with and without TCF are compared for the UDDS driving cycle.

## 2. Vehicle Backward Model

In this paper, analysis on transient fuel consumption was carried out based on the backward model of a Mazda CX9 powered by a conventional gasoline powertrain. The model was then validated with experimental data available from the Argonne National Laboratory (ANL) [20]. The model of HEV was arranged by integrating ECMS, EM, and battery submodels using a P2 mild HEV configuration as shown in Figure 1. The description of the Mazda CX9 conventional vehicle and HEV backward model validation was discussed in [18]. The reader is kindly asked to refer to the work [18] for a detailed description of the model and its submodels.

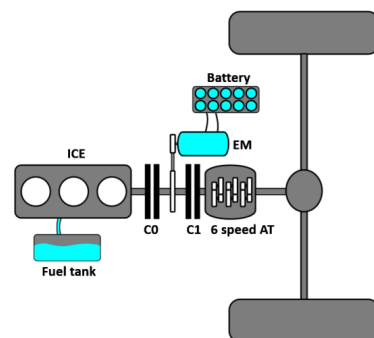


Figure 1. Schematic of the P2 HEV powertrain [18].

The backward model estimates the required torque from the vehicle speed imposed by the drive cycle [3,4]. Having the vehicle speed and its acceleration as inputs from the drive cycle, the required force on the vehicle tire patch  $F_{wheel}$  was calculated as:

$$F_{wheel} = M \cdot \frac{dv}{dt} + F_{aero} + F_{roll} \quad (1)$$

where  $M$  is the vehicle mass,  $F_{aero}$  is the aerodynamic resistance force, and  $F_{roll}$  is the tire rolling resistance. The road gradient forces were neglected as the road is supposed to be horizontal.

The effect of rotational masses, such as tire, crankshaft, and flywheel inertias, were taken into account in the model by adding the inertial torque values in corresponding sub-blocks.

Using vehicle configuration and transmission system parameters (Table 1), the required torque  $T_{req}$  and angular speed  $\omega_{req}$  were calculated based on the force and linear speed of the vehicle.

**Table 1.** Mazda CX9 2016 [18].

| Parameter                                   | Unit           | Variable     | Value  |
|---|----------------|--------------|--|
| Vehicle                                     |                |              |  |
| Vehicle mass                                | kg             | $M$          | 2041   |
| Frontal area                                | m <sup>2</sup> | $A_f$        | 2.4207   |
| Aerodynamic drag coefficient                | -              | $c_x$        | 0.316  |
| Gear ratios                                 | -              | $i_{gb}$     | 1st—3.49; 2nd—1.99;<br>3rd—1.45; 4th—1;<br>5th—0.71; 6th—0.6 |
| Final drive ratio                           | -              | $i_{final}$  | 4.41   |
| Tire size                                   | -              |              | P255/50VR20  |
| Passenger capacity                          |                |              | 7  |
| Internal Combustion Engine                  |                |              |  |
| SAE net torque @ rpm                        | Nm             |              | 310 @ 2000   |
| Fuel System                                 | -              |              | Gasoline direct<br>injection                                 |
| SAE net power @ rpm                         | kW             |              | 169 @ 5000   |
| Displacement                                | L              |              | 2.5  |
| Electric Motor                              |                |              |  |
| Maximum power                               | kW             |              | 27   |
| Maximum torque @ rpm                        | Nm             | $T_{em,max}$ | 65 @ 4000  |
| Battery (Sanyo NCR18650GA Lithium-ion cell) |                |              |  |
| Nominal voltage                             | V              |              | 3.6  |
| Nominal capacity                            | Ah             |              | 3.2  |
| Minimum battery SOC                         | %              | $SOC_{low}$  | 60   |
| Maximum battery SOC                         | %              | $SOC_{high}$ | 80   |
| Operating temperature                       | °C             |              | −20~60   |
| Ambient temperature                         | °C             |              | 20   |
| Battery pack configurations                 | -              |              | 14s12p   |

### 3. Conventional Vehicle Fuel Consumption Model and Its Validation

Once the required torque and speed were evaluated, the engine fuel usage based on a steady-state map was estimated using a lookup table with the linear interpolation method. The steady-state map of the Mazda CX9 SkyActiv engine is shown in Figure 2 based on the experimental data from [21].

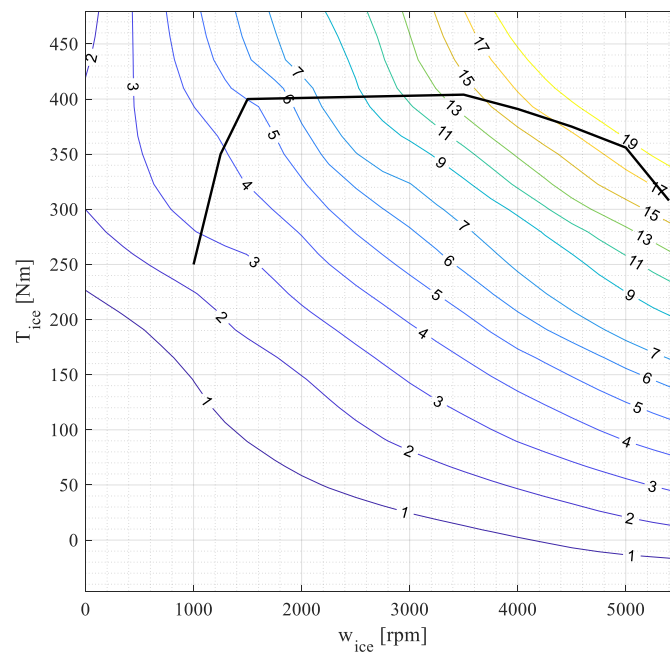


**Figure 2.** Fuel consumption map of Mazda CX9 2016 internal combustion engine obtained in steady-state conditions [18].

The results of the backward model and the experimental tests for fuel consumed during different drive cycles are reported in Table 2. The results contain three cases of fuel consumption: (1) measured experimentally, (2) calculated using steady-state engine map and experimentally measured engine torque  $T_{ice}$  and rotation speed  $\omega_{ice}$  as an input, and (3) calculated using the steady-state engine map and model estimated values of torque and speed. The difference between fuel consumption obtained from the experiments ( $f_{c_{exp}}$ ) and the steady-state fuel consumption  $f_{c_{ss\_exp}}$  based on measured engine torque ( $T_{ice\_exp}$ ) and angular speed ( $\omega_{ice\_exp}$ ) is in the range of 3.7–5.2%. This difference is due to transient characteristics of the engine that the steady-state maps do not cover. The steady-state fuel consumption  $f_{c_{ss\_m}}$  was determined by using the estimated torque and the speed in the backward model. The difference between  $f_{c_{ss\_exp}}$  and  $f_{c_{ss\_m}}$  is in the range of 1–2.4%, which is mainly due to the error in estimating the engine torque and speed.

**Table 2.** Comparison of overall fuel consumption from the model and experiment for the conventional vehicle.

| Driving Cycle | Experimental $f_{c_{exp}}$ | Calculated:<br>Steady-State Map, Experimental<br>Torque and Speed $f_{c_{ss\_exp}}$ | Calculated:<br>Steady State Map, Estimated<br>Torque and Speed $f_{c_{ss\_m}}$ |
|---------------|----------------------------|---|--|
| UDDS          | 741.6 g                    | 712 g   | 695 g  |
| HW            | 787 g                      | 758 g   | 750.6 g  |
| US06          | 1005 g                     | 952 g   | 940 g  |

#### 4. Transient Fuel Consumption Model and Its Validation

To improve the accuracy of the fuel consumption calculation from the backward model, TCF was used to calibrate the steady-state fuel consumption rate of the model ( $\dot{m}_{ss\_m}$ ) with the experimental one ( $\dot{m}_{exp}$ ). As mentioned above in this paper, the transient model was developed based on the approach described in [14]. In that work, three different

representations for TCF were proposed. The most accurate fuel usage estimation was obtained when TCF was represented by the following expression [14]:

$$TCF = A \cdot \omega_{ice} + B \cdot \frac{d\omega_{ice}}{dt} + C \cdot T_{ice} + D \cdot \frac{dT_{ice}}{dt} + E \quad (2)$$

Regression coefficients  $A$ ,  $B$ ,  $C$ ,  $D$ ,  $E$  can be estimated separately for the following use cases:

$$\text{Case (a)} : \frac{d\omega_{ice}}{dt} > 0 \text{ and } \frac{dT_{ice}}{dt} > 0;$$

$$\text{Case (b)} : \frac{d\omega_{ice}}{dt} > 0 \text{ and } \frac{dT_{ice}}{dt} < 0;$$

$$\text{Case (c)} : \frac{d\omega_{ice}}{dt} \leq 0 \text{ and } \frac{dT_{ice}}{dt} > 0;$$

$$\text{Case (d)} : \frac{d\omega_{ice}}{dt} \leq 0 \text{ and } \frac{dT_{ice}}{dt} \leq 0;$$

In [14], it was established that coefficients  $A$ ,  $B$ ,  $C$  and  $D$  have an order of exponential magnitude  $-5$ ,  $-5$ ,  $-4$  and  $-3$  for all the cases, respectively. This means that coefficient  $D$  is the dominant one. That indicates that the torque change rate mostly affects the transient fuel consumption increase. Therefore, TCF can be approximated with good accuracy using the following simplified form of Equation (2):

$$TCF = D \cdot \frac{dT_{ice}}{dt} + E \quad (3)$$

In the current work, coefficient  $E$  was set to one ( $E = 1$ ), so that that TCF was applied only if there was a torque change. Otherwise, TCF was 1, which means that the predicted fuel consumption was equal to the one computed using the steady-state map. Regression analysis was carried out using experimental data on UDDS, US06, and HW driving cycles available on the ANL database [20]. The calculated values of  $T_{ice\_m}$  and  $\omega_{ice\_m}$  from the backward model was used to determine the torque change rate and fuel consumption  $\dot{m}_{ss\_m}$ . Then, TCF was calculated as a ratio of measured  $\dot{m}_{exp}$  and steady-state fuel consumption  $\dot{m}_{ss\_m}$ . Depending on the sign of the  $T_{ice\_m}$ ,  $\omega_{ice\_m}$  changing rate, the data were split into 4 cases. The data sampling time during the experiments was 0.1 s and a moving average filter of order 10 was used for smoothing. Moreover, operating points with low distribution density were excluded from the analysis. In the case shown in Figure 3a, the few operating points with a torque change rate higher than 200 Nm/s were omitted as outliers. The values of coefficient  $D$  derived from this linear regression analysis are shown in Figure 3 and summarized in Table 3. These values of regression coefficient  $D$  are aligned with those obtained in [14].

**Table 3.** The values of coefficient  $D$  obtained from regression analysis.

| Cases | $D$     | $E$ |
|-------|---------|-----|
| (a)   | 0.0026  | 1   |
| (b)   | -0.0003 | 1   |
| (c)   | 0.0033  | 1   |
| (d)   | 0.0011  | 1   |

The fuel consumption obtained from the steady-state map can then be corrected with TCF as:

$$\dot{m}_{TCF} = TCF \cdot \dot{m}_{ss\_m} \quad (4)$$

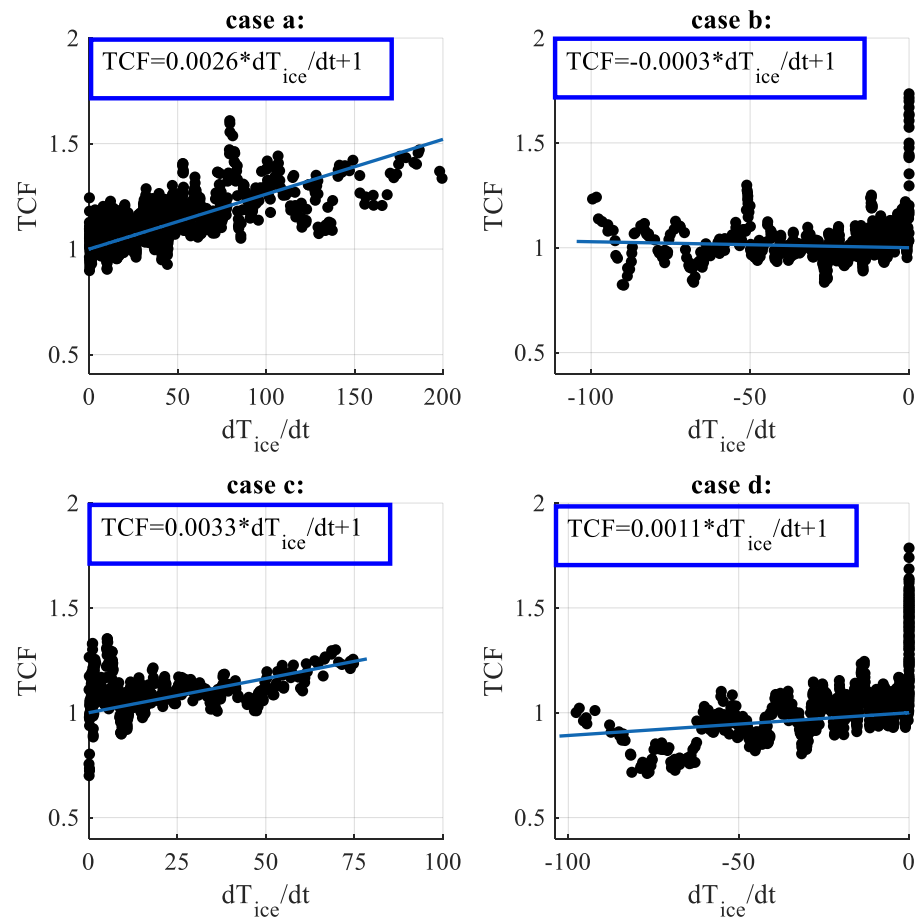


**Figure 3.** TCF vs. torque changing rate of the engine in 4 cases: (a)  $\frac{d\omega_{ice}}{dt} > 0$  and  $\frac{dT_{ice}}{dt} > 0$ ; (b)  $\frac{d\omega_{ice}}{dt} > 0$  and  $\frac{dT_{ice}}{dt} < 0$ ; (c)  $\frac{d\omega_{ice}}{dt} \leq 0$  and  $\frac{dT_{ice}}{dt} > 0$  (d)  $\frac{d\omega_{ice}}{dt} \leq 0$  and  $\frac{dT_{ice}}{dt} \leq 0$ .

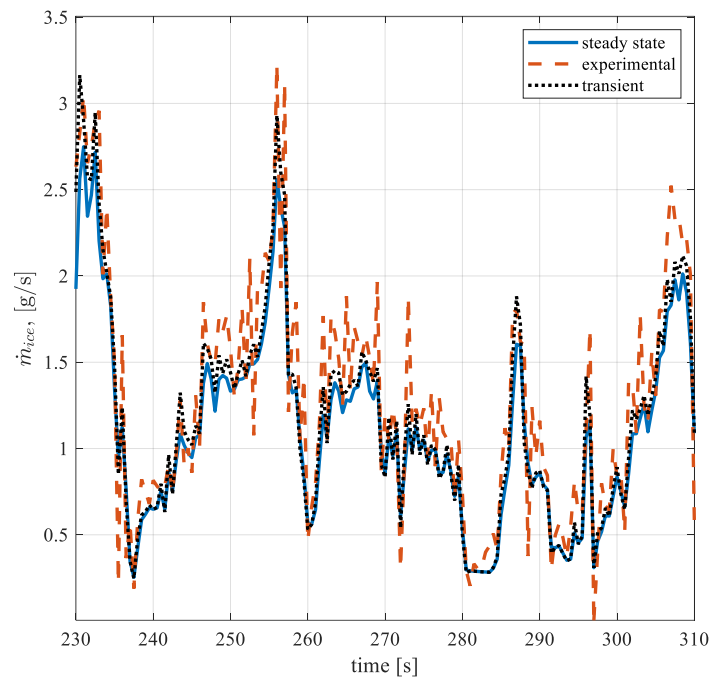
Finally, the developed model with TCF was simulated for three drive cycles. Figure 4 shows plots for  $\dot{m}_{ss\_m}$ ,  $\dot{m}_{exp}$  and  $\dot{m}_{TCF}$  on the UDDS cycle. It can be seen that after introducing TCF, the fuel consumption result of  $\dot{m}_{TCF}$  is more accurate with  $\dot{m}_{exp}$  compared with steady-state prediction.

Figure 5 demonstrates the cumulative sum of the fuel rate:  $f_{c_{ss\_m}}$ ,  $f_{c_{model}}$ , and  $f_{c_{exp}}$  over the cycle. The results show that overall fuel consumption with transient correction ( $f_{c_{TCF}}$ ) and experimental total fuel usage ( $f_{c_{exp}}$ ) were matched better. Thus, it can be concluded that the developed TCF model allows for effectively including the transient characteristics of the engine.

Table 4 summarizes the overall fuel consumption results for different driving cycles. It shows a good fit of  $f_{c_{TCF}}$  with  $f_{c_{exp}}$ . In addition, the last column indicates the difference between  $f_{c_{TCF}}$  and  $f_{c_{ss\_m}}$ , the sum of all extra fuel usage during the transient phases.

**Table 4.** Comparison of total fuel consumption calculated from the model and measured from the experiments.

| Driving Cycle | $f_{c_{exp}}$ | $f_{c_{TCF}}$ | $f_{c_{TCF}} - f_{c_{ss\_m}}$ |
|---------------|---------------|---------------|-------------------------------|
| UDDS          | 741.6 [g]     | 743 [g]       | 51 [g]                        |
| HW            | 787 [g]       | 785 [g]       | 35 [g]                        |
| US06          | 1005 [g]      | 1006 [g]      | 66 [g]                        |



**Figure 4.** Instant fuel consumption rate from the steady-state map, the experiment, and the model including TCF.

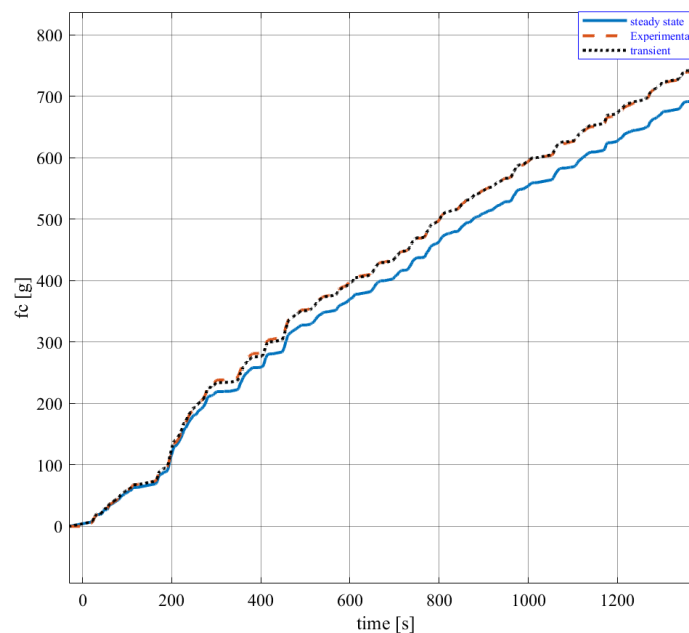


**Figure 5.** Overall fuel consumption of steady-state, experiment, and the model predictions.

## 5. ECMS with Steady-State Map

Equivalent consumption minimization strategy was applied to the system as a supervisory controller which defines the optimum ratio of energy split between EM and ICE. This controller is a real-time controller not requiring preliminary knowledge about the driving cycle. At each time step, the ECMS decides the power split depending on the current situation. Hence, it gives a local minimum because it minimizes the objective function at



each instant. The objective function  $J_{ecms}$  is the sum of the fuel consumption rate of ICE  $\dot{m}_{ice}$  and the equivalent consumption rate of EM  $\dot{m}_{eqv}$  as [15,17,18]:

$$J_{ecms} = \dot{m}_{ice}(P_{ice}) + \dot{m}_{eqv}(P_{bat}) \tag{5}$$

where,  $\dot{m}_{eqv}(P_{bat})$  can be derived by calculating engine fuel used to generate the same power provided by EM considering all the efficiencies of the power flow path.

$$\dot{m}_{eqv}(P_{bat}) = P_{em}(T_{em}, \omega_{em}) \cdot s_{eqv} = T_{em} \cdot \omega_{em} \cdot s_{eqv} \tag{6}$$

Equivalent factor  $s_{eqv}$ :

$$s_{eqv} = \begin{cases} \frac{1}{LHV \cdot \eta_{ice} \cdot \eta_{em} \cdot \eta_{inv} \cdot \eta_{bat}} & (P_{bat} \geq 0) \\ \frac{1}{LHV \cdot \eta_{ice} \cdot \eta_{em} \cdot \eta_{inv} \cdot \eta_{bat}} & (P_{bat} < 0) \end{cases} \tag{7}$$

where  $LHV$  is the lower heating value of the fuel,  $\eta_{ice}$  is the average efficiency of the ICE,  $\eta_{em}$  is the average efficiency of the EM,  $\eta_{bat}$  is the average efficiency of battery and  $\eta_{inv}$  is the average efficiency of the inverter. To reduce calculation time the equivalent factor  $s_{eqv}$  can be evaluated by using mean efficiencies. However, the fuel economy model can be improved even more by using specific efficiencies of each operation point.

The fuel consumption rate of the engine  $\dot{m}_{ice}(P_{ice})$  is approximated as a polynomial with independent variables of engine torque and speed  $T_{ice\_m}$  and  $\omega_{ice\_m}$  from the engine steady-state map of Figure 6.

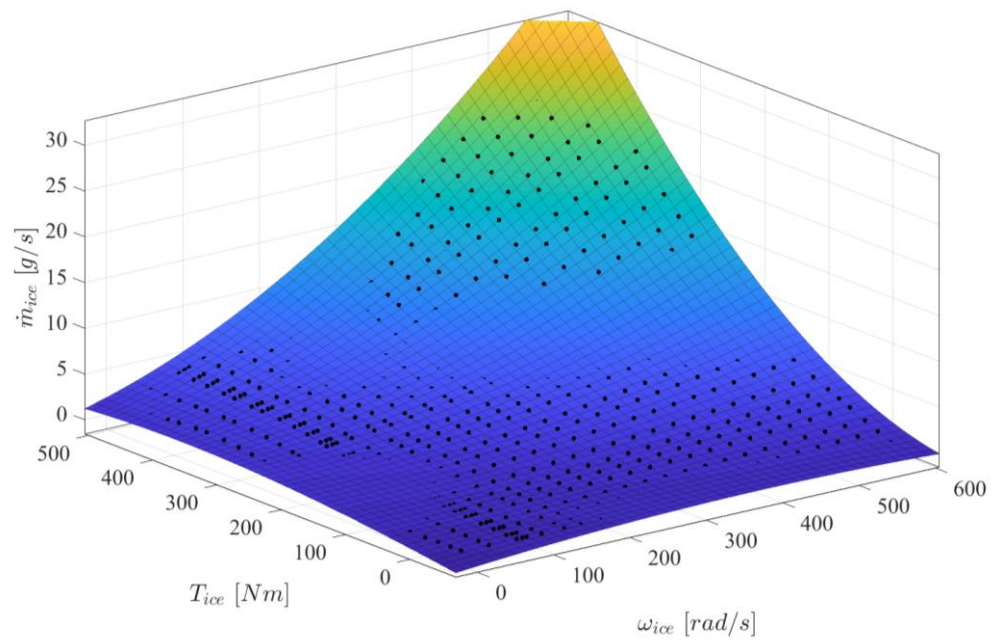


**Figure 6.** Curve fitting of the engine fuel consumption rate by engine torque and rotation speed [18].

The experimental data are approximated by a polynomial fit carried out by means of MATLAB curve fitting toolbox with a good quality  $R^2 = 0.9961$  [18].

To have a fair comparison of the fuel consumption of the HEV system the SOC, of the battery should maintain at the same level at the beginning and the end of the driving cycle. This is usually referred to as the charge sustaining operation mode of HEV. Therefore, the equivalent fuel consumption of the EM is penalized by an S-shaped correction function that varies with SOC. The expression suggested in [14] was utilized in the objective function as shown in Equations (9) and (10). The ECMS controller with the penalization factor and the operational constraints are described in detail in Equations (8) and (11) [18].

The objective function in the ECMS controller is described as:

$$J_{ecms} = \dot{m}_{ice}(P_{ice}) + PF_{soc} \cdot \dot{m}_{eqv}(P_{bat}) \tag{8}$$

where  $PF_{soc}$  is the penalization factor on SOC [17]:

$$PF_{soc} = 1 - 0.15 \cdot \overline{SOC}^3 \tag{9}$$

And normalized battery  $\overline{SOC}$  [17]:

$$\overline{SOC} = \frac{2 \cdot SOC - (SOC_{high} + SOC_{low})}{SOC_{high} - SOC_{low}} \tag{10}$$

The torque split logic between the electric motor and the internal combustion engine must satisfy the following constraints:

$$\begin{aligned} T_{gb} &= (T_{em} \cdot U_{pulley} + T_{ice}) / i_{gb} \\ 0 &\leq T_{ice} \leq T_{ice,max} \\ -T_{em,max} &\leq T_{em} \leq T_{em,max} \end{aligned} \tag{11}$$

The cost function in Equation (8) is two-variables ( $P_{em}$  and  $P_{ice}$ ) nonlinear optimization problem. However, the problem can be reduced to a single variable type by means of the first constraint described in Equation (11). Therefore, a built-in MATLAB function `fminbnd` solver can be used [22]. The above control strategy is first implemented for comparison purposes with objective functions which consider the steady-state fuel consumption rate  $\dot{m}_{ice}(P_{ice})$  without TCF. In Figure 7 the ICE torque, EM torque, and requested torque at the gearbox input are plotted. The values of the torques at a time instant 375 s are indicated using data tips, which show that the sum of ICE and EM torques is equal to the requested torque. Figure 7d shows that a charge sustaining mode is realized by the controller as the SOC at the beginning and end of the driving cycle are at the same level. For the UDDS driving cycle, the overall fuel consumption is about 620.7 g.

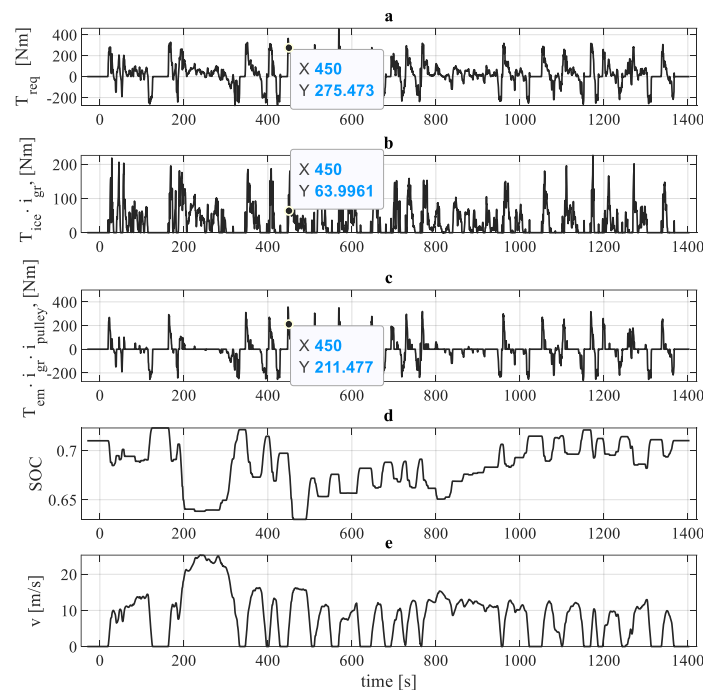


Figure 7. (a) Requested torque, (b) engine torque, (c) EM torque at the gearbox output level, (d) SOC profile under ECMS controller without TCF, and (e) vehicle velocity.

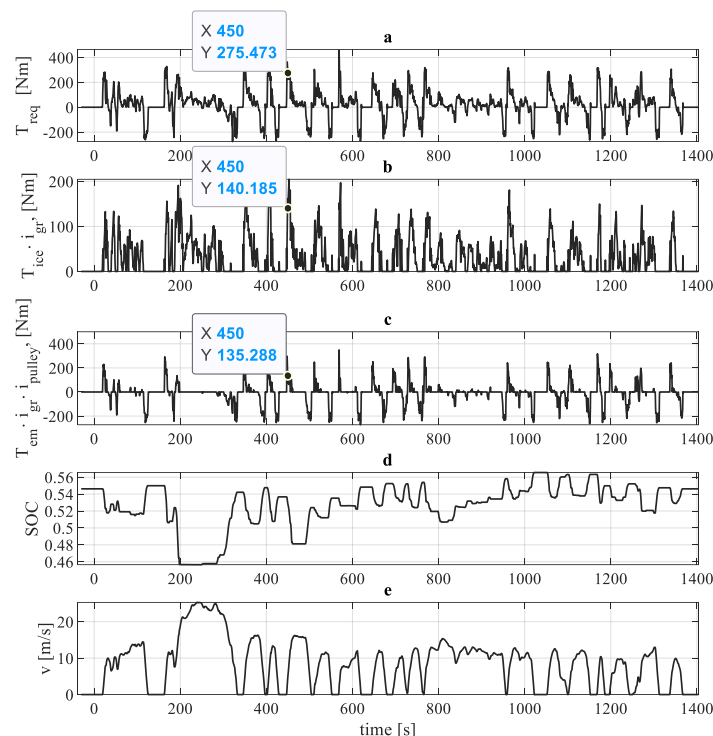
### 6. ECMS with Transient Correction Factor

As discussed above, in transient, the fuel consumption is corrected with the TCF of Equation (4). The introduction of the TCF in the objective function of ECMS penalizes the torque changing rate for ICE, which leads to the ICE operating more steadily than the ECMS based on steady-state fuel consumption only, as in the previous case.

Then the objective function with TCF can be introduced to Equation (8):

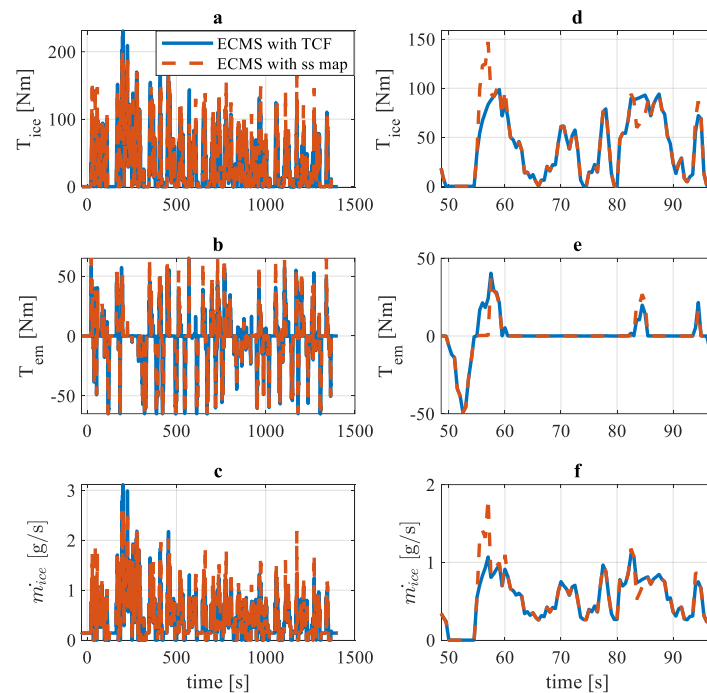
$$J_{ecms} = TCF \cdot \dot{m}_{ice}(P_{ice}) + PF_{soc} \cdot \dot{m}_{eqv}(P_{bat}) \tag{12}$$

Figure 8 reports the values of the torques when TCF is considered and the charge sustaining condition is satisfied. The overall fuel consumption was reduced to 616.3 g, which corresponds to an additional 4.4 g of fuel savings with respect to ECMS with a steady-state map.



**Figure 8.** (a) Requested torque, (b) ICE torque, (c) EM torque at the gearbox output level, (d) SOC profile under ECMS controller with TCF, checking for demand fulfillment by the power sources and charge sustaining operating condition, and (e) vehicle velocity.

Figure 9 shows the torque values of the ICE and EM, and fuel consumption rate values for the two ECMS cases: with and without TCF. The zoom-in to a specific region is shown on the right plot. It can be seen that the engine torque  $T_{ice}$  is smoother for the case with TCF (blue solid line). Due to the influence of TCF in the time interval of 55–57 s, the controller chooses a hybrid mode that minimizes the engine’s high transient operation. Instead, in the case when TCF is not considered (dashed orange line) the pure ICE traction mode is chosen by the controller in the same time range. On the last subplot (Figure 9c), the fuel consumption rate shown highlights the reduction of the fuel consumption rate in the considered time interval. Hence, as the charge sustaining constraint is satisfied, the cumulative fuel consumption is also reduced to the values stated before.



**Figure 9.** Comparison of engine and EM operations under control of ECMS with/without TCF: (a) the engine torque profile, (b) the EM torque profile, (c) fuel consumption rate of the engine, (d) a plot is zoomed in 50–100 s (e) b plot is zoomed in 50–100 s (f) c plot is zoomed in 50–100.

The values of total fuel consumed on three driving cycles using ECMS controller with and without TCF are summarized in Table 5. Because US06 is the most aggressive driving cycle in terms of transients, the largest benefit of 5.1 g fuel saving is achieved with it. In the HW driving cycle, which is characterized by steady driving scenarios instead, the fuel-saving is reduced to 3.2 g. In UDDS, the reduction is 4.4 g. This improvement can be increased further to 8.9 g by doubling battery capacity (14s24p). The increased utilization of electric traction leads to needs on a larger battery.

**Table 5.** Total fuel consumption under ECMS with and without TCF.

| Drive Cycle | ECMS with Steady-State Map | ECMS with TCF | Fuel-Saving |
|-------------|----------------------------|---------------|-------------|
| UDDS        | 620.7 g                    | 616.3 g       | 4.4 g       |
| HW          | 754.2 g                    | 751 g         | 3.2 g       |
| US06        | 922.7 g                    | 917.6 g       | 5.1 g       |

## 7. Conclusions

In the context of vehicle fuel consumption calculation over a drive cycle, it is common to model the engine with steady-state maps. This assumption might lead to a 2–8% underestimation of the fuel consumption for the vehicle with a conventional powertrain compared with experimental results. The fuel consumption during transient is obtained by multiplying a correction factor, whose parameters can be identified from experimental data to the fuel consumption obtained from a steady-state map. The comparison of total fuel consumption on UDDS, US06, and HW driving cycles shows a good match with the experimentally measured data. The simulations for HEV were performed for a P2 off-axis HEV with a battery capacity of 1.8 kWh (14s12p) using an ECMS control strategy. The temperature limitation of the battery pack was not considered. By integrating the obtained TCF model to the objective function of the ECMS, the torque split was modified. This resulted in less transient operations of the engine, as the introduction of TCF penalized the use of the engine in regimes with high torque change rates. Therefore, the transient phases were supported mainly by EM. This

led to a fuel consumption reduction of 0.4–0.7%, depending on the drive cycle, with respect to the case when no transient corrections were accounted for in the controller. However, further improvement of the fuel efficiency could be achieved by considering larger battery capacity. Doubling the battery capacity will reduce the impact of battery limitations. In this case, ECMS with the TCF strategy shows an improvement of 1.4% in fuel economy. In this paper, the thermal constraint of the battery was not considered as in the previous work [18]. For the same 14s12p battery configuration and vehicle, the battery temperature for different drive cycles was within desired operation range. However, in the current work, the developed management strategy, which included transient behavior, allowed the ICE to operate in a stable mode; thus, the EM was exposed to more transient performance. This can increase temperature rise in the battery with respect to ECMS without TCF. This effect could be included in future research.

**Author Contributions:** Conceptualization, G.Y., S.R., E.E., A.T., and N.A.; Data curation, G.Y. and E.E.; Formal analysis, G.Y. and S.R.; Funding acquisition, E.E., A.T., and N.A.; Investigation, G.Y., S.R., and E.E.; Methodology, S.R.; Project administration, G.Y., A.T., and N.A.; Resources, S.R.; Software, G.Y. and S.R.; Supervision, A.T. and N.A.; Validation, G.Y., S.R., and E.E.; Writing—original draft, G.Y.; Writing—review & editing, S.R., E.E., A.T., and N.A. All authors have read and agreed to the published version of the manuscript.

**Funding:** This research received no external funding.

**Institutional Review Board Statement:** Not applicable.

**Informed Consent Statement:** Not applicable.

**Data Availability Statement:** Not applicable.

**Conflicts of Interest:** The authors declare no conflict of interest.

## References

1. Cheli, F.; Gobbi, M.; Holjevac, N. Vehicle subsystems' energy losses and model-based approach for fuel efficiency estimation towards an integrated optimization. *Int. J. Veh. Des.* **2018**, *76*, 46–81. [CrossRef]
2. Amati, N.; Tonoli, A.; Castellazzi, L.; Ruzimov, S. Design of electromechanical height adjustable suspension. *Proc. Inst. Mech. Eng. Part D J. Automob. Eng.* **2018**, *232*, 1253–1269. [CrossRef]
3. Onori, S.; Serrao, L.; Rizzoni, G. *Hybrid Electric Vehicles: Energy Management Strategies*; Springer: London, UK, 2016.
4. Rahman, Z.; Butler, K.; Ehsani, M. A Study of Design Issues on Electrically Peaking Hybrid Electric Vehicle for Diverse Urban Driving Patterns. SAE Technical Paper 1999-01-1151. 1999. Available online: <https://saemobilus.sae.org/content/1999-01-1151/> (accessed on 19 January 2022).
5. Guzzella, L.; Sciarretta, A. *Vehicle Propulsion Systems*; Springer: Berlin/Heidelberg, Germany, 2007.
6. DeKraker, P.; Stuhldreher, M.; Kim, Y. Characterizing Factors Influencing SI Engine Transient Fuel Consumption for Vehicle Simulation in ALPHA. *SAE Int. J. Engines* **2017**, *10*, 529–540. [CrossRef]
7. Bandaru, B.; Rao, L.; Babu, P.; Varathan, K. *Real Road Transient Driving Cycle Simulations in Engine TestBed for Fuel Economy Prediction*; SAE Technical Paper 2014-01-2716; SAE International: Vancouver, BC, Canada. Available online: <https://saemobilus.sae.org/content/2014-01-2716/s> (accessed on 19 January 2022).
8. Bishop, J.; Stettler, M.; Molden, N.; Boies, A.M. Engine maps of fuel use and emissions from transient driving cycles. *Appl. Energy* **2016**, *183*, 202–217. [CrossRef]
9. Lindgren, M. A Transient Fuel Consumption Model for Non-road Mobile Machinery. *Biosyst. Eng.* **2005**, *91*, 139–147. [CrossRef]
10. Ben-Chaim, M.; Shmerling, E.; Kuperman, A. Analytic Modeling of Vehicle Fuel Consumption. *Energies* **2013**, *6*, 117–127. [CrossRef]
11. Zhao, Q.; Chen, Q.; Wang, L. Real-Time Prediction of Fuel Consumption Based on Digital Map API. *Appl. Sci.* **2019**, *9*, 1369. [CrossRef]
12. Zhou, M.; Jin, H. Development of a transient fuel consumption model. *Transp. Res. Part D Transp. Environ.* **2017**, *51*, 82–89. [CrossRef]
13. Guang, H.; Jin, H. Fuel consumption model optimization based on transient correction. *Energy* **2018**, *169*, 508–514. [CrossRef]
14. Mizushima, N.; Yamaguchi, K.; Kawano, D.; Suzuki, H.; Ishii, H. A Study on High-Accuracy Test Method for Fuel Consumption of Heavy-Duty Diesel Vehicles Considering the Transient Characteristics of Engines. *SAE Int. J. Fuels Lubr.* **2016**, *9*, 383–391. [CrossRef]
15. Paganelli, G.; Delprat, S.; Guerra, T.M. Equivalent Consumption Minimization Strategy for Parallel Hybrid Powertrains. In Proceedings of the 55th IEEE Vehicular Technology Conference, Birmingham, AL, USA, 6–9 May 2002; pp. 2076–2081.

16. Hegde, S.; Bonfitto, A.; Rahmeh, H.; Amati, N.; Tonoli, A. Optimal Selection of Equivalence Factors for ECMS in Mild Hybrid Electric Vehicles. In Proceedings of the ASME 2021 International Design Engineering Technical Conferences and Computers and Information in Engineering Conference, ASME, Virtual, 17–19 August 2021. Available online: <https://asmedigitalcollection.asme.org/IDETC-CIE/proceedings-abstract/IDETC-CIE2021/85369/V001T01A019/1128359> (accessed on 19 January 2022).
17. Liu, X.; Qin, D.; Wang, S. Minimum Energy Management Strategy of Equivalent Fuel Consumption of Hybrid Electric Vehicle Based on Improved Global Optimization Equivalent Factor. *Energies* **2019**, *12*, 2076. [[CrossRef](#)]
18. Yakhshilikova, G.; Ezemobi, E.; Ruzimov, S.; Tonoli, A. Battery Sizing for Mild P2 HEVs Considering the Battery Pack Thermal Limitations. *Appl. Sci.* **2021**, *12*, 226. [[CrossRef](#)]
19. Rahmeh, H.; Bonfitto, A.; Ruzimov, S. Fuzzy Logic vs. Equivalent Consumption Minimization Strategy for Energy Management in P2 Hybrid Electric Vehicles. In *Volume 4: 22nd International Conference on Advanced Vehicle Technologies (AVT)*; American Society of Mechanical Engineers: St. Louis, MO, USA, 2020. [[CrossRef](#)]
20. Argonne National Library; Transportation Technology R&D Center. Downloadable Dynamometer Database. 2015. Available online: <https://www.anl.gov/es/energy-systems-d3-2016-mazda-cx9> (accessed on 19 January 2022).
21. Combining Data into Complete Engine ALPHA Maps. Available online: <https://www.epa.gov/vehicle-and-fuel-emissions-testing/combining-data-complete-engine-alpha-maps> (accessed on 19 January 2022).
22. Find Minimum of Single-Variable Function on Fixed Interval. Available online: <https://it.mathworks.com/help/matlab/ref/fminbnd.html> (accessed on 19 January 2022).